

A&A manuscript no.
(will be inserted by hand later)

Your thesaurus codes are:
04.19.1, 04.03.1, 13.25.3

ASTRONOMY
AND
ASTROPHYSICS

The ROSAT All-Sky Survey Bright Source Catalogue

W. Voges, B. Aschenbach, Th. Boller, H. Bräuninger, U. Briel, W. Burkert, K. Dennerl, J. Englhauser, R. Gruber, F. Haberl, G. Hartner, G. Hasinger*, M. Kürster**, E. Pfeffermann, W. Pietsch, P. Predehl, C. Rosso, J.H.M.M. Schmitt***, J. Trümper, and H.U. Zimmermann

Max-Planck-Institut für extraterrestrische Physik, Postfach 1603, 85740 Garching, Germany

Received 1 March 1999 / Accepted 25 June 1999

Abstract. We present the ROSAT All-Sky Survey Bright Source Catalogue (RASS-BSC, revision 1RXS) derived from the all-sky survey performed during the first half year (1990/91) of the ROSAT mission. 18,811 sources are catalogued (i) down to a limiting ROSAT PSPC count-rate of 0.05 cts/s in the 0.1–2.4 keV energy band, (ii) with a detection likelihood of at least 15 and (iii) at least 15 source counts. The 18,811 sources underwent both an automatic validation and an interactive visual verification process in which for 94% of the sources the results of the standard processing were confirmed. The remaining 6% have been analyzed using interactive methods and these sources have been flagged. Flags are given for (i) nearby sources; (ii) sources with positional errors; (iii) extended sources; (iv) sources showing complex emission structures; and (v) sources which are missed by the standard analysis software. Broad band (0.1–2.4 keV) images are available for sources flagged by (ii), (iii) and (iv). For each source the ROSAT name, position in equatorial coordinates, positional error, source count-rate and error, background count-rate, exposure time, two hardness-ratios and errors, extent and likelihood of extent, likelihood of detection, and the source extraction radius are provided. At a brightness limit of 0.1 cts/s (8,547 sources) the catalogue represents a sky coverage of 92%. The RASS-BSC, the table of possible identification candidates, and the broad band images are available in electronic form (Voges et al. 1996a) via <http://wave.xray.mpe.mpg.de/rosat/catalogues/rass-bsc>.¹

Key words: catalogs - surveys - X-rays: general

Send offprint requests to: W. Voges (wvoges@mpe.mpg.de)

* Present address: Astrophysikalisches Institut Potsdam, An der Sternwarte 16, 14482 Potsdam, Germany

** Present address: ESO–La Silla, Alonso de Cordova 3107, Vitacura, Casilla 19001, Santiago 19, Chile

*** Present address: Hamburger Sternwarte, Gojenbergsweg 112, 21029 Hamburg, Germany

¹ The RASS-BSC and the identification table are also available in electronic form at the CDS via anonymous ftp to cdsarc.u-strasbg.fr (130.79.128.5) or via <http://cdsweb.u-strasbg.fr/Abstract.html>

1. Introduction

Sky surveys play a major role in observational astronomy, in particular in the era of multi-wavelength observations. Before the launch of the ROSAT satellite several all-sky X-ray catalogues existed based on collimated counter surveys (see Table 1). One of the main scientific objectives of ROSAT was to conduct the first all-sky survey in X-rays with an imaging telescope leading to a major increase in sensitivity and source location accuracy (Trümper 1983). Actually, the ROSAT mirror system (Aschenbach 1988) and the Position Sensitive Proportional Counter (PSPC) (Pfeffermann et al. 1988) used for the survey were primarily optimized for detecting point sources in the all-sky survey. However, the wide angle and fast optics as well as the low detector background of the PSPC provided excellent conditions for studying extended sources like supernova remnants, clusters of galaxies, and the diffuse X-ray background. In this context the “unlimited field of view” of the all-sky survey was of great advantage.

The ROSAT All-Sky Survey (RASS) was conducted in 1990/91, just after the two month switch-on and performance verification phase. The first processing of the ROSAT All-Sky Survey took place in 1991–1993 resulting in about 50,000 sources. This source list had not been published, because during the analysis a large number of minor deficiencies and possibilities for improvement were discovered. Nevertheless, the data have been extensively used by the scientific groups at MPE and their collaborators for many scientific projects.

Based on the experience with the first RASS processing a second analysis was performed in 1994–1995, resulting in 145,060 sources (detection likelihood ≥ 7). The present publication comprises only the brightest 18,811 of this sample. These data represent by far the most complete and sensitive X-ray sky survey ever published. It is a factor of 20 more sensitive than any previous all-sky survey in X-rays and contains about a factor of 4 more sources than all other X-ray catalogues, which sample only a few percent of the sky.

In this paper we present the outcome of the RASS in terms of “point sources”. For 98.2% of the 18,811 sources

Satellites	date	energy range (keV)	number of sources	References
UHURU	1970-73	2-6	339	Forman et al. (1978)
OSO-7	1971-73	1-60	184	Markert et al. (1979)
ARIEL-5 ($ \text{b}^{\text{II}} > 10^\circ$)	1974-80	2-18	142	McHardy et al. (1981)
ARIEL-5 ($ \text{b}^{\text{II}} < 10^\circ$)	1974-80	2-10	109	Warwick et al. (1981)
HEAO-1/A1	1977-79	1-20	842	Wood et al. (1984)
HEAO-1/A2	1977-79	0.2-2.8	114	Nugent et al. (1883)
HEAO-1/A4	1977-79	13-180	40	Levine et al. (1984)

Table 1. X-ray astronomy missions and all-sky surveys before the launch of ROSAT.

the source extent radius is less than 5 arcmin, and for 99.6% the extent is smaller than 10 arcmin. 0.4% of the sources exhibit a larger source extent and show complex emission patterns (see Section 3.2) rather than a point-like spatial distribution. These sources have been included for completeness as they fulfill the selection criteria of the RASS-BSC (hereafter RBSC). Diffuse sky maps with angular resolution of 40 arcmin and diffuse sky maps in six colours of 12 arcmin resolution have been published elsewhere (Snowden et al. 1995, 1997).

In Sect. 2 we summarize the basic properties of the ROSAT All-Sky Survey and of the Standard Analysis Software System (hereafter SASS). The selection strategy for including sources into the RBSC, the screening process, and the content of the RBSC are presented in Sect. 3. The results from the correlation of RBSC sources with various databases are given in Sect. 4. The electronic access to the RBSC is described in Sect. 5.

2. The ROSAT All-Sky Survey

2.1. Observation strategy and exposure map

ROSAT has conducted the first All Sky Surveys in soft X-rays (0.1–2.4 keV; 100–5 Å) and the extreme ultraviolet (0.025–0.2 keV; 500–60 Å) bands using imaging telescopes (Trümper 1983, Aschenbach 1988, Wells et al. 1990, Kent et al. 1990). The satellite was launched on June 1, 1990 and saw first light on June 16, 1990 (Trümper et al. 1991). The following 6 week calibration and verification phase already included a small fraction of the sky survey (see Table 2). The main part of the survey began on July 30, 1990 and lasted until January 25, 1991. A strip of the sky which remained uncovered, because of operational problems in January, was retrieved in February and August 1991 (see Table 2). The data obtained until 1991 form the basis of the present analysis. The total survey exposure time amounts to $1.031 \cdot 10^7$ s or 119.36 days.

The basic survey strategy of ROSAT was to scan the sky in great circles whose planes were oriented roughly perpendicular to the solar direction. This resulted in an exposure time varying between about 400 s and 40,000 s at the ecliptic equator and poles respectively. During the passages through the auroral zones and the South Atlantic Anomaly the PSPC had to be switched off, leading to a

Dates		ROSAT days	Detector
1990 Jul 11 - 1990 Jul 16		41– 45	PSPC-C
1990 Jul 30 - 1991 Jan 25		60–242	PSPC-C
1991 Feb 16 - 1991 Feb 18		263–264	PSPC-B
1991 Aug 03 - 1991 Aug 13		435–444	PSPC-B

Table 2. ROSAT All-Sky Survey observation intervals.

decrease of exposure over parts of the sky (see Fig. 1). The sky coverage as a function of the exposure time is displayed in Fig. 2. For exposure times larger than 50 seconds the sky coverage is 99.7% for the observations until 1991.

2.2. SASS processing

The first analysis of the all-sky survey data was performed for strips of $2^\circ \times 360^\circ$ containing the data taken during two days. These strips were analysed using various source detection algorithms, comprising two sliding window techniques (differing in how the background was determined) and a maximum-likelihood method. A list of X-ray sources (RASS-I) was produced which included information about sky position and source properties, such as count-rate, hardness-ratios, extent, and source detection likelihoods. The main aim of this analysis was to supply almost immediate information about the X-ray sources and to allow a fast quality check of the survey performance.

The RBSC presented in this paper is based on the so-called RASS-II processing which is described below in Sect. 2.2.1–2.2.3.

2.2.1. Advantages of the RASS-II processing

The main differences between the RASS-II data processing and the RASS-I processing are as follows: (i) the photons were not collected in strips but were merged in 1,378 sky-fields of size $6.4^\circ \times 6.4^\circ$, so that full advantage was taken of the increasing exposure towards the ecliptic poles; (ii) neighbouring fields overlapped by at least 0.23 degrees, to ensure detection of sources at the field boundaries, which posed a problem in the first processing; (iii) a new aspect solution reduced the number of sources with erroneous position and morphology; (iv) the calculation of

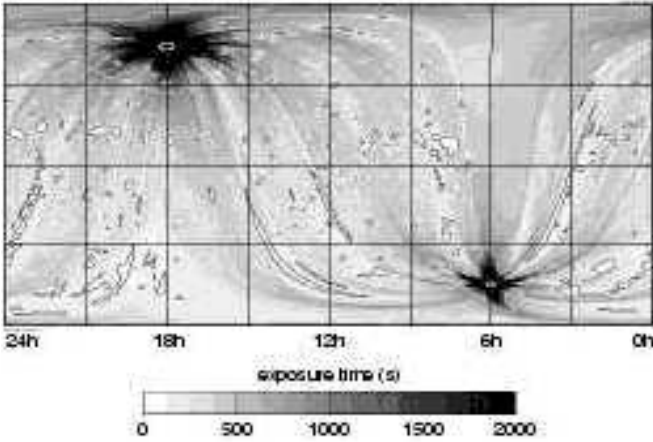


Fig. 1. Exposure map after the second processing of the ROSAT All-Sky Survey data, displayed in equatorial coordinates / rectangular projection. The spatial resolution of the map is 900 arcsec. Contours are drawn at 100s, 1000s, and 10000s, respectively. Due to the survey scan law the ecliptic poles (at R.A.= 6 h and R.A. = 18 h) received the highest exposure. The southern hemisphere on average received less exposure due to missed data during South Atlantic Anomaly passages. At some locations in the sky (seen as white spots) there were not enough guide stars for the automatic measuring and control system of the satellite.

the spline-fitted background map was improved, resulting in better determined count-rates; (v) the candidate list for the maximum-likelihood analysis (see Sect. 2.2.2) was enlarged by lowering the threshold values for the two preceding sliding window source detection algorithms, and by changing the acceptance criteria to allow very soft and very hard sources to be included; and (vi) photons obtained with poor aspect solutions were no longer accepted.

2.2.2. Source detection algorithm

The source detection algorithms of the SASS processing can be divided into 6 different steps:

1. The local-detect method

The local-detect algorithm is based on a sliding window technique. It was already successfully used for the analysis of EINSTEIN data and has been modified for ROSAT. A window of 3×3 pixels is moved across the binned photon images. These images are produced by binning the data into 512 by 512 pixel images with a pixel size of 45 arcsec for three energy bands (broad: Pulse Height Amplitude (PHA) channels 11–235 (0.1–2.4 keV), soft: channels 11–41 (0.1–0.4 keV), hard: channels 52–201 (0.5–2.0 keV)). The contents of the pixels inside the detection cell are added and compared with the local background taken from the 16 pixels surrounding the 3×3 pixel detection window. To detect also extended sources the size of the

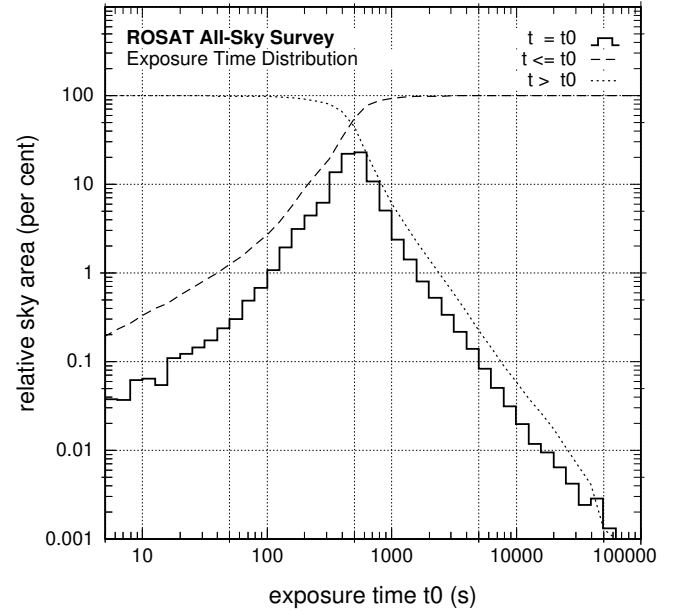


Fig. 2. Differential and cumulative exposure time distribution for the second processing of the ROSAT All-Sky Survey. The time bins are equidistantly spaced logarithmically. The histogram shows the fraction of the sky covered with exposure time t_0 . The dashed and dotted lines show the fraction of the sky with exposure time less than t_0 or greater than t_0 , respectively. The statistics were derived from the all-sky exposure map shown in Fig. 1 (resolution $15'$). For most of the sky (97%) the exposure time was more than 100 s. The regions around the ecliptic poles received the highest exposure: 27 square degrees received more than 10,000 s and 135 square degrees received less than 5 s.

detection cell is increased systematically by keeping the ratio of the areas of background and source windows fixed at 16/9.

2. The background map

Using the source list produced in three energy bands by the local-detect method, circular regions are cut out around each source position. The radius of the circle is dependent on the detection cell size. The resulting “swiss-cheese”-images are fitted by a two-dimensional spline function to fill the holes and to generate three energy dependent background maps. In Fig. 3 we show the background maps in the soft and hard energy bands in galactic coordinates.

3. The map-detect algorithm

The map-detect algorithm produces a second source list by repeating the sliding window search, using a 3×3 pixel window and the spline fit to the background. Again sources are searched for in three energy bands and with varying cell size.

4. Merging of source lists

The source lists from the local- and map-detection algorithms are merged and are further used as input lists to steps 5 and 6.

5. Determination of source extraction radius

A preliminary extent of the source counts is derived from the radial distribution of counts in annuli centered on the source position. This extent, with a minimum being fixed at 300 arcsec, is baselined as an extraction radius for the selection of the photons used in the subsequent maximum-likelihood detection algorithm.

6. The maximum-likelihood method

The merged source lists are used as input to the maximum-likelihood method (Craddock et al. 1987). In contrast to the previously described detection algorithms this method takes into account the position of each individual photon. This allows a proper weighting of each photon with the instrument point spread function, which is a strong function of off-axis angle. The high-resolution photons in the center of the PSPC are weighted higher than the off-axis photons. The maximum-likelihood method provides a source position and existence likelihood in the broad band. With this position fixed, the detection likelihood in each of the 4 energy bands A (PHA channels 11–41), B (52–201), C (52–90), D (91–201) is calculated. Vignetting is taken into account for each photon using an analytic fit, leading to a mean vignetting factor for each source. Source extent and its likelihood are derived using just the broad band data, assuming that the point response function and the surface brightness are 2-D Gaussian functions, that they are independent of photon energy, and that the background is uniform in annular rings concentric around the optical axis.

For strong sources various techniques are applied in the SASS to quantify the likelihood for time variability and to perform spectral fits. This information is not included in the present version of the RBSC.

2.2.3. Parameters derived from the RASS-II processing

In the following section a few basic source parameters from the RASS-II processing are described. A complete description of the derived source parameters is given at <http://wave.xray.mpe.mpg.de/rosat/documentation/productguide> and a description of the catalogue entries of the RBSC is available at

<http://wave.xray.mpe.mpg.de/rosat/catalogues/rass-bsc>.

A source count-rate corrected for vignetting is given in the broad band. Two hardness ratios HR1 and HR2 are calculated, which represent X-ray colours. From the source counts in the band A and the band B HR1 is given by: $HR1=(B-A)/(B+A)$. HR2 is determined from the source counts in the bands C and D by: $HR2=(D-C)/(D+C)$. Since background subtraction is involved, the

source counts in some bands may be negative. These negative counts have been set to zero, so that HR1 or HR2 becomes -1 or $+1$. Note that HR2 is a hardness ratio constructed in the hard region, since bands C and D together contain the same channels as the hard band B. Thus HR1 near -1 and HR2 near $+1$ is no contradiction. Hardness ratio errors greater than 9.99 have been set to 9.99.

Each source has been assigned a 'priority' parameter, the leftmost 6 characters of which denote the detection history before the maximum-likelihood algorithm was applied. These are: 1=M-broad, 2=L-broad, 3=M-hard, 4=L-hard, 5=M-soft, 6=L-soft. Here M and L stand for the map-detect algorithm and the local-detect method, respectively. Broad, hard and soft refer to the energy bands defined above. A flag is set to 0 for no detection or 1 for detection.

The source extent (**ext** in the RBSC) is defined as the excess above the width of the point spread function given in arcsec. In addition, the likelihood (**ext1**) for the source extent and the extraction radius in arcsec for a source (**extr**) used in the maximum-likelihood method are provided.

3. The ROSAT Bright Source Catalogue

3.1. Selection criteria

The total number of sources found in the RASS II is 145,060 (detection likelihood ≥ 7). From this database the RBSC was selected according to the following criteria: (i) the detection likelihood is ≥ 15 ; (ii) the number of source photons is ≥ 15 and (iii) the source count-rate in the (0.1–2.4 keV) energy band is ≥ 0.05 counts s^{-1} , resulting in 23,394 sources. These sources underwent an intensive screening process, which is described in the following section.

3.2. Screening process

In order to ensure a high quality of the catalogue, the images of all sources which fulfill the above mentioned criteria were individually inspected.

An automatic as well as a visual screening procedure was applied to all 1,378 sky fields. The automatic procedure searched for sources with overlapping extraction radii, as the count-rate determination can be affected in such cases. These sources were colour-coded in the subsequent visual inspection process.

The visual inspection process is based on ROSAT All-Sky Survey images in the broad, soft and hard energy bands. The SASS position for each RBSC source as well as the extraction radius were marked in the various images. This enables the identification of regions on the sky where the detection algorithm had split sources into multiple detections, and verifies that the source extraction radius and the source position are correct. In addition, sources which were missed by the detection algorithm can

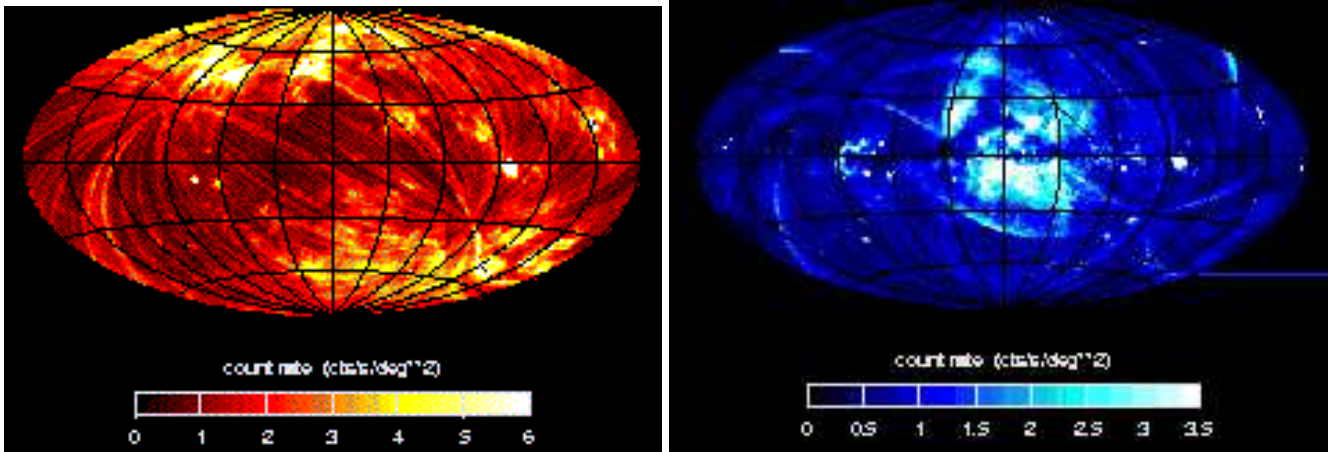


Fig. 3. Soft (left) and hard (right) background images in galactic coordinates. The intensity is colour-coded.

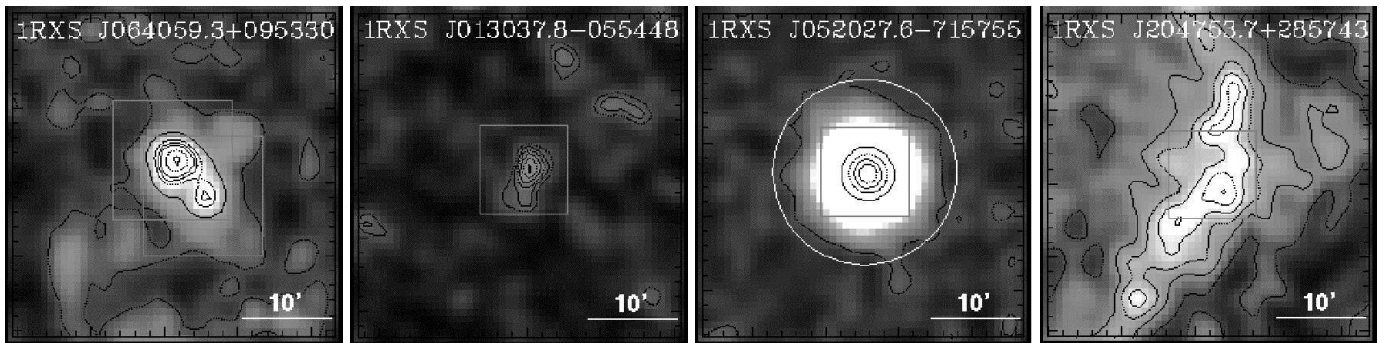


Fig. 4. Examples for sources with warning flags. X-ray contour lines are overlaid on the broad-band images. The SASS extraction radius is defined by the green rectangles and the new extraction radius, when determined, is shown by the white circle around the source position. From left to right: **1:** SASS flux determination affected by nearby sources; **2:** Possible problem with position determination; **3:** Source extent larger than SASS extraction radius; **4:** Complex diffuse emission pattern.

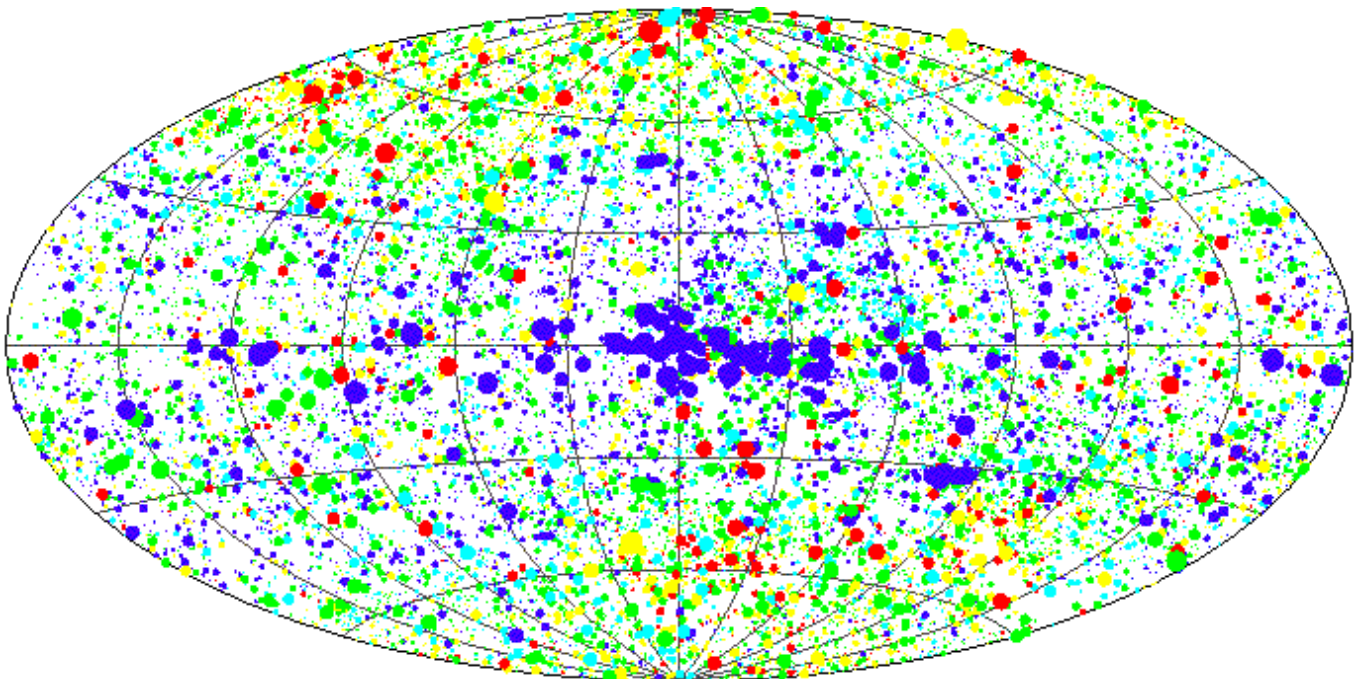


Fig. 5. Aitoff projection of the distribution of all RBSC sources obtained in the ROSAT All-Sky Survey observations until August 13, 1991 in galactic coordinates. The size of the symbols scales with the logarithm of the count-rate and the colours represent 5 intervals of the hardness ratio HR1: red ($-1 < \text{HR1} < -0.6$); yellow ($-0.6 < \text{HR1} < -0.2$); green ($-0.2 < \text{HR1} < 0$); cyan ($0 < \text{HR1} < 0.2$); blue ($0.2 < \text{HR1} < 0.6$).

be found. During the visual screening process source parameters from the SASS could be checked interactively, using software tools from the Extended Scientific Analysis System (EXSAS, see Zimmermann et al. 1994). The reliability of the screening process was verified in different ways. 100 of the 1,378 sky fields were used as training sets for the screening process and were analysed by more than one person to minimize the deviations in the flag setting. The results of the flag setting were again visually inspected.

About 16% of the 23,394 sources were found to be spurious detections (mainly in large extended emission regions like the Vela Supernova remnant and the Cygnus Loop) which have been removed from the final source list. The remaining 18,811 sources are included in the present version of the RBSC. For 94% of these sources the SASS parameters were confirmed, and the remaining 6% of the sources have been flagged. The source flags applied to RBSC sources are defined in the following paragraphs (see Fig. 4 for examples of flagged RBSC sources).

(i) **nearby flag**

This flag is set when the distance between two sources is less than the sum of the individual extraction radii. The count-rate might be wrong in such cases. The **nearby flag** is given to both sources, when their count-rate ratio is less than a factor of 5. If one source exhibits a count-rate which is at least 5 times higher than that of the weaker source, the nearby flag is given only to the weaker source. In such cases, the count-rate of the brighter source is not affected significantly. The nearby flag was given to 588 sources.

(ii) **position error**

Whenever the source position is obviously not centered on the source extraction cell the position flag is applied. We did not correct the positions as there may be several different reasons for this problem (e.g. asymmetric elongated emission patterns, multiple emission maxima in the detection cell). The **position error** flag was applied to 317 sources and a broad band image provided for each one.

(iii) **source extent larger than the source cell size extraction radius.**

The standard analysis software fails in some cases to find the correct source extent, with the result that the count-rates are usually underestimated. All of these marked sources underwent a post-processing step to quantify whether the source extent is indeed larger than the value found by the standard analysis software. The number of sources marked with the **source extent flag** was 225. A broad band image is available for inspection and the new extraction radius is indicated by a white circle.

(iv) **complex emission patterns**

The SASS count-rate as well as the source position may be uncertain for sources which show complex emission patterns. 177 sources were flagged in the visual process. The flag serves as a warning that the SASS count-rate and po-

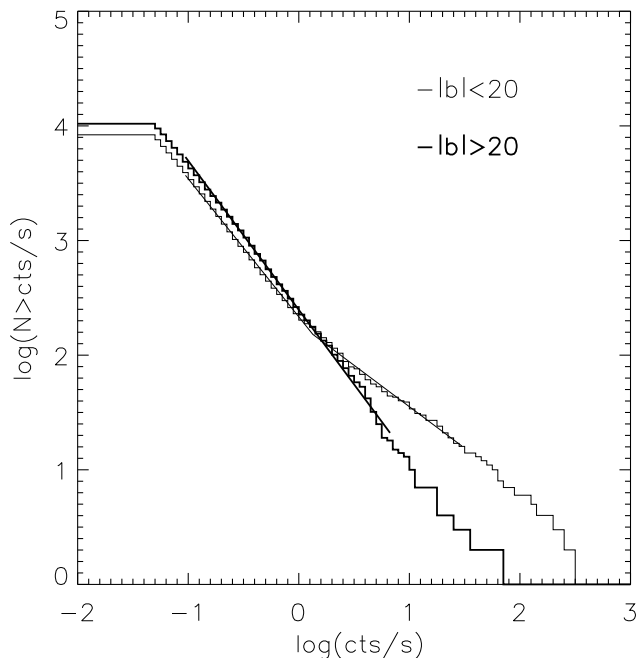


Fig. 6. Histogram of the cumulative number density ($N > \text{cts/s}$) of RBSC sources in the galactic plane ($|b| < 20^\circ$) and outside the galactic plane ($|b| > 20^\circ$), plotted against broad band count-rate.

sition may be uncertain. A broad band image is available for inspection.

(v) **Sources missed by the detection algorithm**

In the visual inspection process sources were found, which were missed by the standard analysis software system. The number of such sources included into the RBSC is 49. Their main parameters, count-rate, exposure time, and position were determined in an interactive process using EXSAS tools.

3.3. Statistical properties

3.3.1. Sky- and count-rate distributions

In Fig. 5 we present the sky distribution of all RBSC sources in galactic coordinates. The size of the symbols scales with the logarithm of the count-rate and the colours represent 5 intervals of the hardness ratio HR1. The distribution of RBSC sources shows the clustering of the bright ($> 1.3 \text{ counts s}^{-1}$) hard X-ray sources in the galactic plane, well known from the UHURU and HEAO-1 sky surveys. At fainter count-rates ($\leq 1.3 \text{ counts s}^{-1}$) the source distribution is more uniform. This is illustrated in Fig. 6, where we compare the cumulative number count distributions for sources in the galactic plane ($|b| < 20^\circ$) and outside the galactic plane ($|b| \geq 20^\circ$). A linear fit to the distribution of all sources outside the galactic plane (thick line in Fig. 6) results in a slope of -1.30 ± 0.03 . The faint line in Fig. 6 represents the count-rate distribution for the

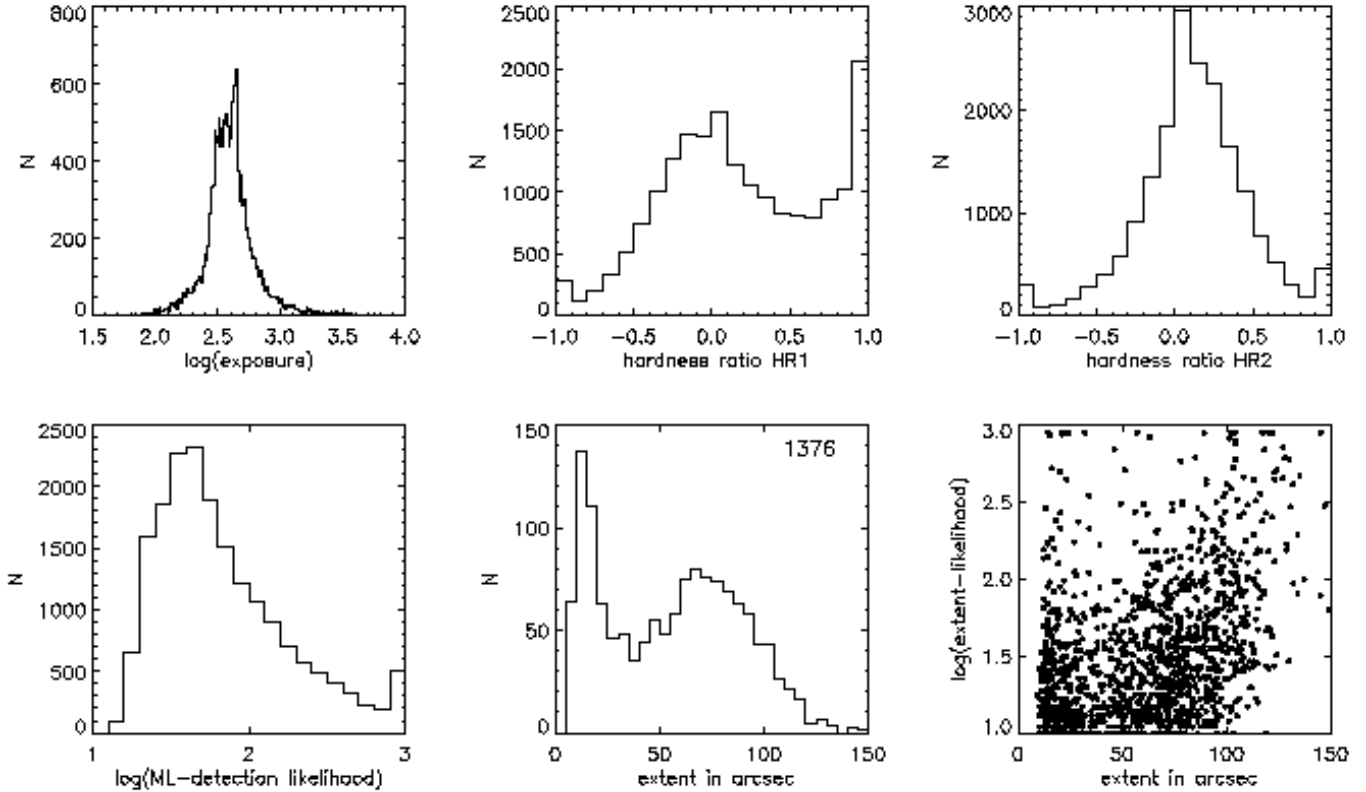


Fig. 7. Six histograms summarizing some results of the analysis of the 18,811 RBSC sources. The upper panel shows the distributions of exposure time, hardness ratios HR1 and HR2. The lower panel displays the distributions of the source detection likelihood and the source extent, and a plot of the extent likelihood against extent. The last two plots are shown for sources which have an extent likelihood ≥ 10 .

galactic plane population of RBSC sources. The histogram shows a break at a count-rate of about $1.3 \text{ counts s}^{-1}$. A linear fit to the distribution above this break-point gives a slope of -1.20 ± 0.04 ; the slope below the break-point is -0.72 ± 0.06 . The flattening of the $\log N$ - $\log(\text{count-rate})$ of the galactic plane distribution at the bright end is due to the disk population of bright X-ray sources (see Fig. 5). The effect of interstellar photoelectrical absorption is demonstrated in Fig. 5 by the fact that sources near the galactic plane exhibit higher values of the hardness ratio HR1 (blue symbols) than sources outside the galactic plane. Although both galactic and extragalactic objects show a large spread in their spectral energy distribution in the ROSAT band (e.g. when simple power-law models were fit to the ROSAT spectra of broad and narrow line Seyfert 1 galaxies, the photon indices ranged between about 2 and 5), the dominant effect here is probably the larger amount of absorption within the galactic plane.

3.3.2. Exposure time, hardness ratios, detection likelihood and source extent distributions

In Fig. 7 we present the distributions of some source parameters of the RBSC. For most of the sources (see the

upper left diagram) the exposure time is of the order of a few hundred seconds. The HR1 and HR2 distributions of the RBSC sources binned in intervals of 0.1 are shown in the upper middle and right diagrams, respectively. This gives a more detailed representation of the HR1 distribution compared to Fig. 5, where only 5 bins were used. The distribution of the source detection likelihood is shown in the lower left diagram. The lower value of 15 is set by the source selection criterion for RBSC sources. The last two diagrams show the distribution of the source extent and the extent-likelihood as a function of extent. A more detailed discussion of the RBSC source parameter distribution for different object classes can be found in Sect. 4.

3.3.3. Positional accuracy

The RBSC sources were correlated with the TYCHO catalogue (Høg et al. 1998) to assess the positional accuracy. As TYCHO contains only stars, this correlation gives the positional accuracy of point-like sources. Figure 8 shows the result from the correlation of the RBSC for a search radius up to 120 arcsec with the TYCHO catalogue entries. The comparison shows that 68% (90%) of the RBSC

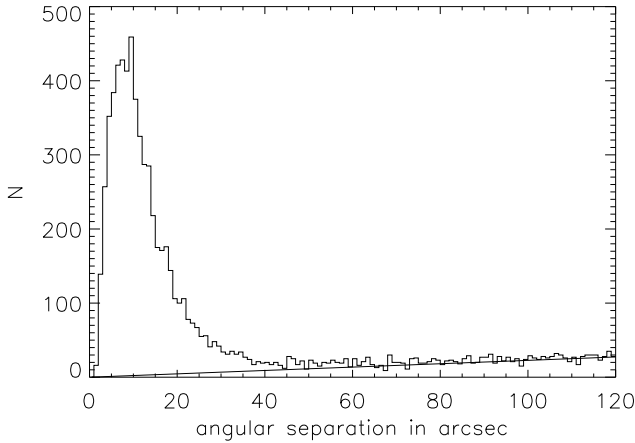


Fig. 8. The plot shows the distribution of the angular separation of RBSC positions from positions of the TYCHO catalogue for bright stars with a positional error of less than 1 arcsec. 68% (90%) of the ROSAT sources are found within 13 arcsec (25 arcsec) of the optical position. The straight line indicates the chance coincidences, demonstrating that for distances ≥ 40 arcsec no reliable ID candidates can be found.

sources are found within 13 arcsec (25 arcsec) of the optical position.

3.3.4. Temporal variability of RBSC sources

We have investigated the temporal variability of RBSC sources on time scales of months to years by comparing the ROSAT All-Sky Survey observations with public pointed ROSAT PSPC observations (see also Voges & Böller 1998). The comparison was done with a search radius of 60 arcsec around the RBSC source position. The resulting number of RBSC sources which have counterparts in ROSAT public pointed observations is 2,611. Figure 9 shows the ROSAT survey count-rate versus the pointing count-rate for these sources. Sources showing a factor of variability above 5 (109), were visually inspected, similar to the screening process performed for the RBSC sources described in Section 3.2, to ensure the reliability of the source existence and of the source count-rate. 20 RBSC sources exhibit a factor of variability between 10 and 100. 5 RBSC sources show a factor of variability above 100. There is an excess of sources with factors of variability above 10, which are brighter during the RASS observations. This is most probably due to the fact, that during the RASS observations the count-rate threshold for the source detection is on average higher with respect to ROSAT pointed observations. As a result, the RBSC sources shown in Fig. 9 are biased towards sources with extreme variability. A comprehensive variability analysis of ROSAT sources will be presented elsewhere.

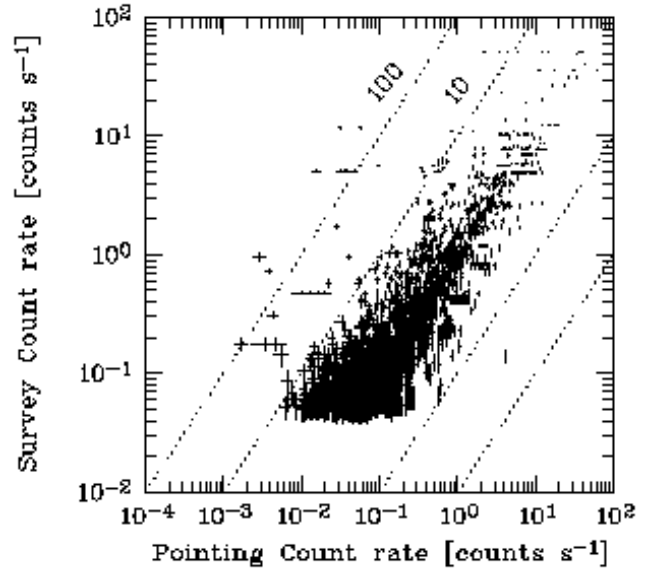


Fig. 9. Count-rate of RBSC sources versus count-rate of corresponding pointed PSPC observations (0.1–2.4 keV). Dashed lines are for fixed factors of variability.

3.3.5. Flux determination and log N–log S distributions

In order to facilitate the use of the catalogue for statistical studies it may be useful to quote not only count-rates but photon fluxes. To convert count-rates into fluxes in the 0.1–2.4 keV energy range we have used two different models: Model 1 assumes a power law $E^{-\Gamma+1} dE$ and may be useful for AGN and clusters of galaxies. We use a fixed photon index of $\Gamma = 2.3$, which is the typical value derived from ROSAT observation of extragalactic objects (see Hasinger et al. 1991, Walter & Fink 1993), and an absorbing column density fixed at the galactic value along the line of sight (Stark et al. 1992). These fluxes, corrected for galactic absorption, are called flux1. Model 2 is based on an empirical conversion between count-rates and fluxes following Schmitt et al. (1995), originally developed to obtain flux values for stars:

$$\text{flux2} = (5.3 \cdot \text{HR1} + 8.31) \cdot 10^{-12} \cdot \text{counts s}^{-1} [\text{erg cm}^{-2} \text{s}^{-1}]$$

Both flux values are listed in the electronic form of our catalogue.

For a statistical study we use both fluxes for three types of objects, stars from the TYCHO catalogue, clusters of galaxies (ACO) from the compilation of Abell et al. (1989) and AGN listed in the Veron catalogue. We have further subdivided the samples in two categories; A: point sources having an extent-likelihood value of zero; B: sources with an extent-likelihood > 0 .

In Fig. 10 we compare the two different flux determinations for the three object classes mentioned above which fall into category A. For TYCHO stars we obtain the largest dispersion between the two methods (left plot in

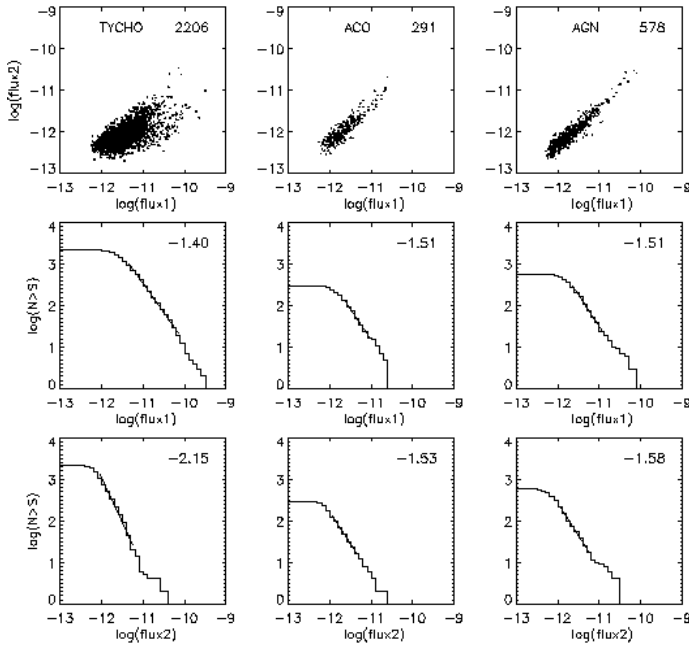


Fig. 10. Nine histograms summarizing the comparison of two different methods for the determination of fluxes and $\log N$ – $\log S$ distributions for point sources (extent-likelihood = 0); first column: TYCHO-stars, second column: clusters of galaxies, third column: active galactic nuclei. The upper panel shows the correlation of flux2 with flux1, the middle panel shows the $\log N$ – $\log(\text{flux1})$ distribution, and the lower panel shows the $\log N$ – $\log(\text{flux2})$ distribution. The number of sources and fitted slope values are inserted.

the upper panel). The differences in fluxes are most likely due to the correction for the galactic absorption. The first method tends to overestimate the flux, as the galactic hydrogen column density is taken along the full line of sight. The true value is lower than the value taken in the computation of flux1. For stars the flux determination with method 2 is more reliable than method 1. A much smaller dispersion is found in comparing flux 1 and flux 2 for ACO and AGN. This is probably explained by the fact that both source populations are detected at high galactic latitudes, where the amount of galactic absorption is considerably smaller than in the galactic plane.

In Fig. 11 we compare the two different flux methods for the three object classes which fall into category B. Again, for TYCHO stars we obtain the largest dispersion between the two methods (left plot in the upper panel). The differences in fluxes are due most likely to the correction for the galactic absorption. As in Fig. 10, a smaller dispersion is found for ACO and AGN objects.

The $\log N$ – $\log S$ distributions for the three object classes of category A are shown in the middle panel (using flux1 values) and in the lower panel (using flux2 values) of Fig. 10. We want to stress that we did not apply any corrections

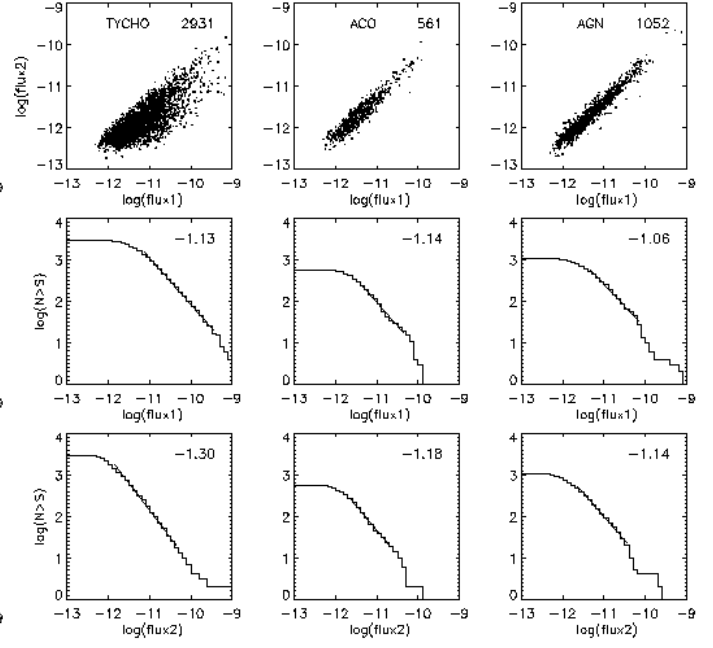


Fig. 11. Nine histograms summarizing the comparison of two different methods for the determination of fluxes and $\log N$ – $\log S$ distributions for point-like and extended sources (extent-likelihood > 0); first column: TYCHO-stars, second column: clusters of galaxies, third column: active galactic nuclei. The upper panel shows the correlation of flux2 with flux1, the middle panel shows the $\log N$ – $\log(\text{flux1})$ distribution, and the lower panel shows the $\log N$ – $\log(\text{flux2})$ distribution. The number of sources and fitted slope values are inserted.

concerning the varying sensitivity of the survey to the $\log N$ – $\log S$ distributions. To determine the slope a linear fit was made to the distribution, starting at the turn-over point of the distribution and ending where the cumulative number count dropped below 15. For ACO and AGN we derive slopes of the $\log N$ – $\log S$ distribution close to -1.5 , which is the expected slope for an Euclidean source distribution, for both flux determination methods. For stars the $\log N$ – $\log S$ distribution is unreliable for flux1 as discussed before. The flux2 distribution for stars (lower panel) is very steep for category A. We have no good explanation for this steep slope. This requires further investigation.

The $\log N$ – $\log S$ distribution for the three object classes of category B are shown in the middle (using flux1 values) and lower panels (using flux2 values) of Fig. 11. The $\log N$ – $\log S$ distributions and their slopes for ACO and AGN objects are comparable with each other for both object types and both flux determination methods.

However, there is a general difference in the slopes for category A and category B sources. For example, the slope for ACO is -1.51 in category A (extl = 0) and -1.14 in category B (extl > 0). There are various explanations possible for the flatter $\log N$ – $\log S$ distribution, such as: a)

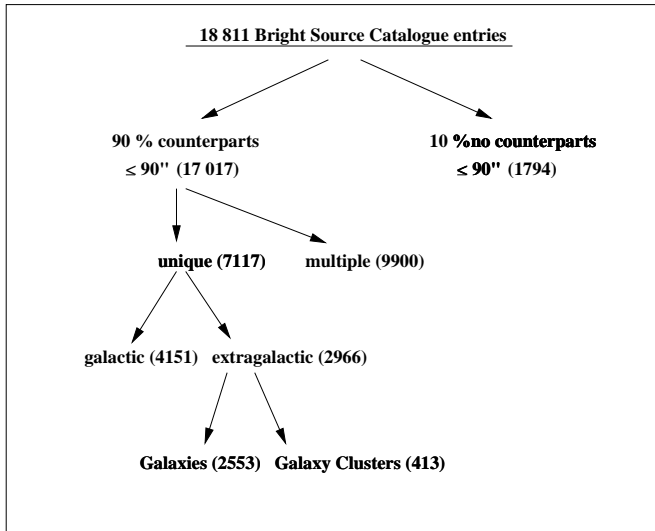


Fig. 12. Diagram showing the distribution and selection of counterparts detected by cross-correlations with catalogues in different wavelength domains.

the count-rate determination for extended sources is underestimated by the SASS; this effect is largest for the fainter X-ray sources; b) the source detection probability for faint extended sources decreases more rapidly than for point sources; c) the probability to assign an extent likelihood value to a detected source decreases with decreasing source count-rate. This effect is stronger for faint extended sources as compared to point-like sources.

Cases a,b and c are well-known software deficiencies in SASS. Various methods have been developed by Böhringer et al. (1998) (growth curve method), DeGrandi et al. (1997) (steepness ratio technique), Ebeling et al. (1993) (Voronoi, tessellation and percolation method), and Wiedenmann et al. (1997) (Scaling index method), to attack this problem, in particular for the study of clusters of galaxies.

4. Correlation with existing data bases

We have performed a cross-correlation of the RBSC with various catalogues. These catalogues include public data bases like the NED or SIMBAD and the latest versions of published catalogues or catalogues in print, as well as lists which were made available to us by private communications from the following alphabetically listed authors: Alcalá et al. (1995, 1996, 1998) (T-Tauri stars), Appenzeller et al. (1998) (optical identifications of northern RASS sources), Bade et al. (1998) (The Hamburg/RASS Catalogue of optical identifications), Berghöfer et al. (1996) (OB-stars), Beuermann et al. (1999) (identification of soft high galactic latitude RASS X-ray sources), Boller et al. (1998) (IRAS galaxies), Buckley et al. (1995), Burwitz et al. (1996a, 1996b) (individual stellar and cataclysmic variables candidates), Covino et al. (1997), Dan-

ner (1998) (stellar candidates in star forming regions), Fleming (1998), Fleming et al. (1995, 1996), (EINSTEIN extended medium sensitivity survey as well as white dwarf and M dwarf detections), Gregory & Condon (1991), Gregory et al. (1996) (radio sources), Haberl et al. (1994), Haberl & Motch (1995) (intermediate polars), Hakala et al. (1993) (cataclysmic variable sources), Harris et al. (1994) (EINSTEIN catalogue of IPC sources), Schwöpe et al. (1999) (identifications of RBSC sources), Hoffleit & Warren (1991) (WFC Bright source catalogue), Hünsch et al. (1998a, 1998b, 1999) (bright and nearby giant, subgiant and main-sequence stars), Kock (1998), Kock et al. (1996), Krautter et al. (1997), Kunkel (1997) (T-Tauri stars), Laurent-Muehleisen et al. (1998) (spectroscopic identification of AGN in the RASS-Green Bank catalogue), Law-Green et al. (1995), Magazzu et al. (1997) (T-Tauri stars), Mason et al. (1992) (white dwarfs), Metanomski et al. (1998) (photometry of F, G and K stars in the RASS), Motch et al. (1996, 1997a, 1997b, 1998) (Galactic plane survey), Nass et al. (1996) (Hamburg catalogue of bright source identifications), Neuhäuser et al. (1995, 1997) (T-Tauri stars), Perlman et al. (1996) (BL Lacertae objects), Romer et al. (1994) (clusters of galaxies), Schmitt (1997) (A, F and G stars in the solar vicinity with distances less than 13 pc), Schmitt et al. (1995) (K and M stars in the solar vicinity with distances less than 7 pc), Staubert et al. (1994) (cataclysmic variable sources), Stern et al. (1995) (RASS identifications in the Hyades cluster), Thomas et al. (1996, 1998) (optical identification of RASS sources), Wagner et al. in preparation (BL Lacertae objects), Wei et al. in preparation (quasars), Wichmann et al. (1996, 1997) (T-Tauri stars), Xie et al. (1997) (active galactic nuclei). These catalogues result in significant measure from follow-up optical observations of ROSAT sources. In these many campaigns extensive use was made of the COSMOS (MacGillivray and Stobie (1985); Yentis et al. (1992)) and APM (McMahon & Irwin (1992)) digitised sky surveys.

Table 3 is a compilation of all catalogues used. In the identification process discussed in this section we use a search radius of 90 arcsec around the RBSC position. For 90% of all RBSC sources at least one counterpart has been found in either one of the catalogues (not taking into account ROSATP3, ROSAT-WGA, and ROSHRI pointing catalogues), whereas 10% have no catalogue entries. We have divided the RBSC sources with catalogue counterparts into two subclasses, (i) unique entries and (ii) multiple entries (see Fig.12). Unique entries refer to RBSC sources which have only one catalogue entry in the various catalogues, or which have a unique identification in the private catalogues. The number of RBSC sources which have unique entries is 7,117. Only these sources are used in the following to derive observational properties, like the ratio of the optical- to X-ray flux. For 9,900 RBSC sources more than one counterpart is detected within the 90 arcsec search radius. RBSC sources with multiple entries are not included in the discussion below. From the 7,117 unique

CATALOGUE	Entries	<300'' all	<300'' near.	search rad.(sr)	bkg. cont.	rad. 68%	rad. 90%	rad. 95.5%	all ≤sr	near. ≤sr	References
SIMBAD	956370	26931	11687	82	9.09	18	47	65	12637	8221	CDS, France (1998)
NED	~ 800000	38675	9103	108	17.31	20	60	86	15873	6826	Helou et al. (1995)
TYCHO	1058332	16737	10274	42	3.63	12	21	28	6156	5465	Høg et al. (1998)
FIRST	437429	7678	2516	58	15.74	16	42	51	1544	978	White et al. (1997)
NVSS	1814748	23991	11544	44	12.83	18	33	39	3594	3437	Condon et al. (1998)
VERON	15106	1936	1826	76	0.77	11	20	27	1718	1701	Veron-Cetty & Veron (1998)
RITTER	414	155	155	46	2.52	8	17	26	149	149	Ritter & Kolb (1998)
PRIVATE	13483	10790	7744	102	0.17	9	17	24	10676	7699	see Sect. 4
ROSATP3	82325	11106	3631	86	5.89	23	48	65	6677	3300	Voges et al. (1996b) (*)
ROSAT-WGA	68907	9451	3057	120	7.51	28	58	80	6624	2908	White et al. (1994) (*)
ROSHRI	7622	3801	869	112	4.83	14	33	52	2682	844	ROSAT RRA consortium (1999) (*)
ROSAT-WFC	688	605	436	92	1.23	24	47	60	593	429	Mason et al.(1995), Pye et al. (1995)
EUVE	549	322	319	98	4.01	49	68	80	308	307	Bowyer et al. (1996)
IRAS-FSC	173044	4049	3711	62	3.70	21	37	48	2205	2200	Moshir et al. (1989)
IRAS-PSC	245889	3923	3300	58	5.86	19	38	50	1566	1562	IRAS Cats. & Atlases Suppl. (1988)

CATALOGUE	Entries	<60'' all	<60'' near.	search rad.(sr)	bkg. cont.	rad. 68%	rad. 90%	rad. 95.5%	all ≤sr	near. ≤sr	References
HST-GSC	25239690	26216	12352	24	13.92	11	18	22	15824	9759	Lasker et al. (1990)

Table 3. List of catalogues used in the correlation with the RBSC. The first column gives the name of the catalogue and the second gives the number of entries. The third and fourth columns show the number of *all* detected counterparts and the total number of the nearest detected counterparts, both found within a search radius of 300 arcsec (90 arcsec for HST-GSC). The following two columns denote the search radii (sr, in arcsec) used for the identifications, as well as the respective background contamination (given in per cent) which may lead to spurious detections. The next 3 columns give the search radii for detection at confidence levels of 68, 90 and 95.5 percent. Columns 10 and 11 present the number of *all* detected counterparts and the nearest neighbours within the search radius (sr). The last column gives the references to the appropriate catalogues. NED is the NASA/IPAC Extragalactic Database, NVSS stands for the NRAO VLA Sky Survey. Private contributions are summarized with PRIVATE and are described in Sect. 4 and in the references. ROSATP3 denotes the ROSAT PSPC-Pointing catalogue by Voges et al.; ROSAT-WGA is the ROSAT PSPC-Pointing catalogue by White, Giommi & Angelini; ROSHRI denotes the ROSAT Result Archive (RRA) catalogue of HRI-Pointings; ROSAT-WFC summarizes the ROSAT Wide Field Camera all-sky survey and the respective optical identifications; EUVE is the second Extreme Ultra-Violet Explorer Catalogue. The IRAS Faint source catalogue and the IRAS Point source catalogue are abbreviated with IRAS-FSC and IRAS-PSC, respectively. The Hubble Guide Star Catalogue is quoted as HST-GSC. ((*) available at <http://wave.xray.mpe.mpg.de/rosat/catalogues/>)

entries 42% are classified as extragalactic objects and 58% are of galactic origin. The extragalactic objects are subdivided into galaxies, including active and non-active galaxies, and clusters of galaxies. 2,553 RBSC sources are identified as galaxies and 413 as galaxy clusters.

The ratio of the X-ray-to-optical flux is a useful discriminant of the nature of the X-ray source, in particular in discriminating between stars and extragalactic objects. Figure 13 shows a correlation of the flux ratio with the optical magnitude for a sample of RBSC sources already identified as stars, AGN, or clusters of galaxies. The gap between stars and AGN/ACO is partly an artifact as star catalogues become incomplete at $m_v > 12$.

In Fig. 14 we compare results of the analysis of RBSC sources for Tycho stars, clusters of galaxies and active galactic nuclei. The distribution of ACO objects show a strong increase towards larger HR1 values, i.e. the majority of ACO objects are much harder as compared to stars and AGN. The AGN show a flat distribution in the range

between -0.5 to $+1.0$. Below $HR1 = -0.5$ the distribution drops quite rapidly due to galactic absorption and due to an intrinsic dispersion in the slopes of the X-ray continua. The HR1 distribution for stars peaks at $HR1 = 0$. Most of the stars are found in the range -0.5 to $+0.5$. The histograms of the hardness ratio HR2 confirm the nature of ACO clusters as “hard” sources. The distribution for stars and AGN are softer and alike. In the distribution of HR2 versus HR1 ACO are dominating the upper right region; AGN are found mostly in the central part with $HR1 > -0.5$ and $-0.5 < HR2 < +0.5$. Stars are occupying a slightly more extended region than AGN. The scatter plot of f_x/f_{opt} versus HR1 shows that the locus of stars is well separated from AGN and ACO clusters. Stars are primarily found in the lower portion of the plot. ACO clusters occupy only the upper right part of the figure. The first histogram in the lower panel of Fig. 14 displays the angular separation of RBSC positions from the optical positions. For stars and AGN most X-ray sources are found

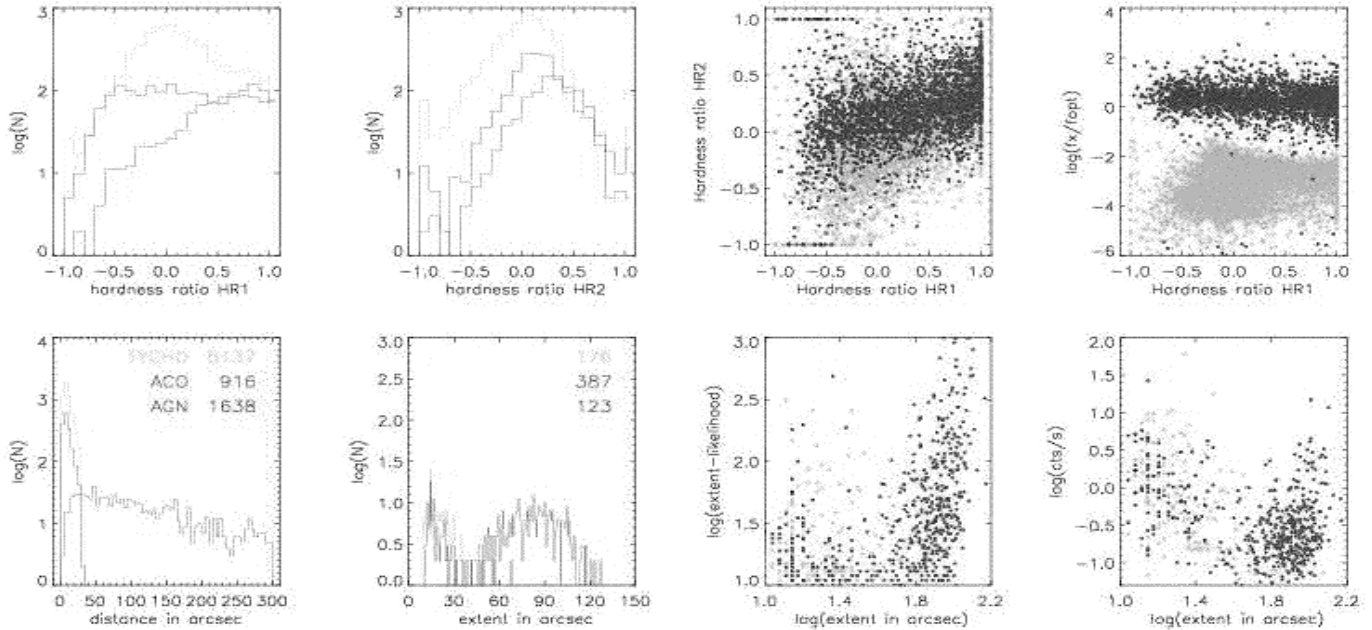


Fig. 14. Eight histograms summarizing some results of the analysis of the RBSC sources for 5,137 TYCHO stars (in green), 916 Abell clusters of galaxies (ACO) (in blue), and 1,638 active galactic nuclei and quasistellar objects of the VERON catalogue (AGN) (in red). The upper panel shows the distributions of the spectral hardness ratios HR1 and HR2, correlations of HR2 with HR1, and f_X/f_{opt} with HR1. The lower panel shows the distribution of the angular separation of RBSC positions from the optical positions, source angular extent, correlations of the extent likelihood and the count-rate with extent. The last three plots are shown for sources which have an extent likelihood ≥ 10 .

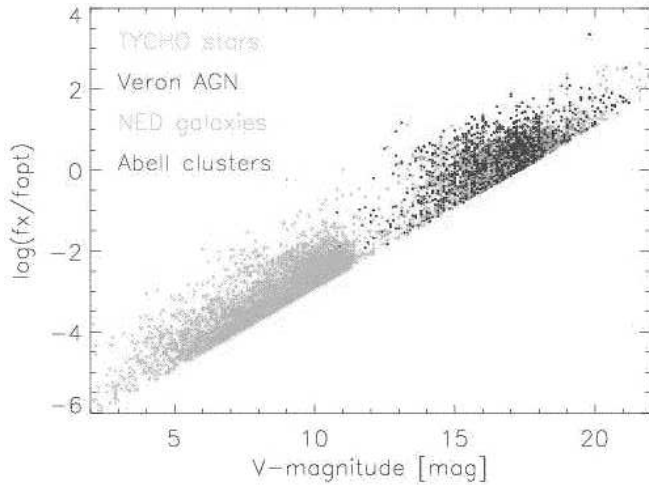


Fig. 13. Ratio of X-ray to optical flux f_X/f_{opt} versus optical magnitude m_V for RBSC sources with unique identification candidates. f_X/f_{opt} was calculated from the 0.1–2.4 keV count-rate and m_V : $\log(f_X/f_{\text{opt}}) = \log(\text{PSPC counts/s} \cdot 10^{-11}) + 0.4 m_V + 5.37$ (Maccacaro et al. 1988). Objects with unique identification are colour-coded: stars (green), active galactic nuclei (red), galaxies (yellow) and clusters of galaxies (blue). Due to the X-ray count-rate limit of $0.05 \text{ counts s}^{-1}$ (flux limit of $5 \cdot 10^{-13} \text{ erg cm}^{-2} \text{ s}^{-1}$) there is a sharp lower boundary in the distribution.

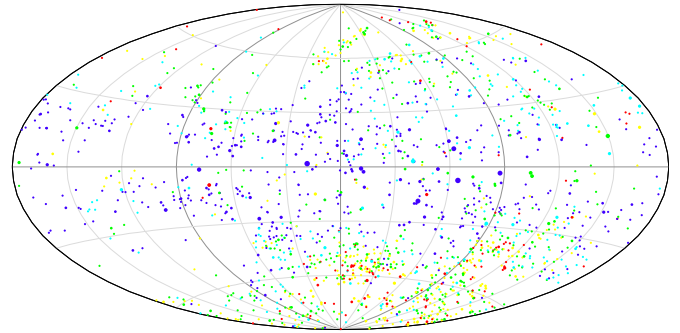


Fig. 15. All-sky distribution in galactic coordinates (Aitoff projection) of RBSC sources which have no identification within a search radius of 90 arcsec, using the catalogues of Table 3. The size of the symbols scales with the logarithm of the count-rate and the colours represent 5 intervals of the hardness ratio HR1: red ($-1 \leq \text{HR1} < -0.6$); yellow ($-0.6 \leq \text{HR1} < -0.2$); green ($-0.2 \leq \text{HR1} < 0.2$); blue ($0.2 \leq \text{HR1} < 0.6$) and violet ($0.6 \leq \text{HR1} \leq 1.0$).

ROSAT All-Sky Survey Bright Source Catalogue (1RXS)

Selection Criteria:

Field of view: lon = 82.5000 d, lat = -69.0000 d, radius = 15.0000 d
(equatorial coordinates; equinox 2000.0)

The list contains 399 sources.

SrcNam	R.A.	Dec.	?p	npedm	riv.	src-cps	?src-cps	bgr-cpsa	exp	hr1	?hr1	hr2	?hr2	ext	extl	srcl	extr	PriFlgE	vigf	orgdat	moddat	#id	field-id	src#	#
1RXS J025613.6-801240	44.05667	-80.21125	12	---	---	7.915E-02	1.954E-02	1.282E-03	303	-0.09	0.22	-0.88	0.32	0	0	32	300	111111b	0.74	960614	000000	2	33031002_0088	1	
1RXS J025613.8-790808	44.05750	-79.13570	12	---	---	6.183E-02	1.726E-02	1.334E-03	281	0.52	0.26	-0.24	0.31	7	1	25	300	111100b	0.72	960614	000000	0	33031002_0074	2	
1RXS J030303.9-783619	45.76625	-78.60542	21	---	---	6.199E-02	1.828E-02	1.409E-03	256	0.59	0.24	0.09	0.32	17	1	18	300	111100b	0.73	960614	000000	4	33031003_0060	3	
1RXS J030343.2-761608	45.93000	-76.26889	12	---	---	8.823E-02	1.333E-02	1.052E-03	657	0.70	0.13	-0.02	0.16	29	6	76	300	111110b	0.73	960614	000000	6	33031003_0019	4	
1RXS J030344.4-775222	45.93500	-77.87292	25	---	---	1.378E-01	2.672E-02	1.333E-03	259	0.93	0.18	0.50	0.18	64	15	30	300	111100b	0.73	960614	000000	2	33031003_0044	5	
1RXS J030618.8-652109	46.57833	-65.35250	21	---	---	3.086E-01	6.514E-02	1.828E-03	95	-0.09	0.19	0.42	0.27	0	0	39	300	111111b	0.65	960614	000000	3	33029004_0011	6	
1RXS J030630.2-753103	46.62584	-75.51750	11	---	---	5.237E-02	9.478E-03	1.178E-03	795	0.77	0.17	0.02	0.18	14	1	59	300	111100b	0.76	960614	000000	2	33030003_0085	7	
1RXS J031033.5-641202	47.63958	-64.20069	18	---	---	1.426E-01	4.344E-02	1.894E-03	106	0.02	0.29	0.21	0.41	11	1	20	300	111010b	0.69	960614	000000	3	33028005_0151	8	
1RXS J031159.8-765131	47.99917	-76.85861	10	---	---	1.838E-01	2.420E-02	1.137E-03	367	0.87	0.09	-0.07	0.13	7	1	138	300	111100b	0.68	960614	000000	5	33031003_0029	9	
1RXS J031250.0-680915	48.20833	-68.15417	15	---	---	1.214E-01	2.948E-02	1.415E-03	193	-0.19	0.20	-0.62	0.44	0	0	28	300	111111b	0.74	960614	000000	1	33029004_0060	10	
1RXS J031557.4-772312	48.98917	-77.38667	13	---	---	1.040E-01	2.389E-02	1.273E-03	260	-0.41	0.17	0.08	0.34	11	1	40	300	111011b	0.76	960614	000000	8	33031003_0033	11	
1RXS J031739.5-663303	49.41459	-66.55083	12	7	---	5.785E-02	1.616E-02	1.115E-03	271	1.00	0.19	0.39	0.30	14	1	33	300	111100b	0.77	960614	000000	33	33029004_0035	12	

Description of the columns:

Col	abbreviation	description
1	SrcNam	the ROSAT All-Sky Survey Catalogue source name
2	R.A.	Right Ascension (2000) in decimal degrees
3	Dec.	Declination (2000) in decimal degrees
4	?p	the total positional error (1σ -radius) in arcsec, including 6" systematic error
5	npedm	screening flags ('T' for 'true', 'F' or '-' for 'false', '.' for 'not used') with the following denomination: n for nearby sources affecting SASS flux determination, p for possible problem with position determination, e for source extended beyond SASS extraction radius, d for complex diffuse emission pattern, m for source missed by SASS
6	riv.	additional flags which are abbreviated with: r source counts and extraction radius recalculated, i for broad band image available, v for variability flag (not yet filled); . is a dummy flag
7	src-cps	source count-rate (vignetting corrected) in the broad band in counts/sec
8	?src-cps	error of source count-rate in the broad band in counts/sec
9	bgr-cpsa	background count-rate (vignetting corrected) in counts/sec/arcmin ²
10	exp	exposure time in sec
11	hr1	hardness ratio 1 (as explained in Sect. 2.2.3.)
12	?hr1	error of hardness ratio 1
13	hr2	hardness ratio 2 (as explained in Sect. 2.2.3.)
14	?hr2	error of hardness ratio 2
15	ext	source extent in arcsec
16	extl	likelihood of source extent
17	srcl	likelihood of source detection defined as $srcl = -\ln(1 - P)$ (P = probability of source existence)
18	extr	extraction radius in arcsec
19	PriFlgE	priority flags derived from the sliding window detection history using either the background map (M) or the local background (B) where 0 = no detection and 1 = detection with the order of flags: M-broad, L-broad, M-hard, L-hard, M-soft, L-soft; E indicates the PHA range with highest detection likelihood (as explained in Sect. 2.2.2.)
20	vigf	vignetting factor
21	orgdat	date (yymmdd) when the source was included
22	moddat	date (yymmdd) when the source properties were changed
23	# id	number of possible identification objects found within a search radius of 5 arcmin
24	field-id src#	the identification number of the SASS field, and the SASS source number
25	#	running source number

Fig. 16. Truncated sample output of a RBSC search inquiry with indicated coordinates and search radius (via the ROSAT source browser).

within 30 arcsec; the distribution for clusters of galaxies is much broader as one would expect from the X-ray source extent alone, which is shown in the next histogram. Abell et al. (1989) determined the cluster centers visually quoting typical standard deviations of $\pm 2'$ - $3'$ for the coordinates with the positional uncertainty depending on the compactness of the cluster. The optically determined centers do not necessarily follow the gas distribution and thus the gravitational potential well, which is the origin of the X-ray emission. Ebeling et al. (1993) found that the optical position of rich clusters had a mean deviation from the RASS position of $3'$ for rich clusters, and $7'$ for poor clusters. In some exceptional cases angular separations of up to $15'$ were found. The last two scatter plots of Fig. 14 exhibit the extent likelihood and the count-rate versus extent. The populations of stars and AGN are well separated from those of ACO clusters.

Figure 15 gives the celestial distribution of RBSC sources which have no counterparts according to the catalogues listed in Table 3, when a search radius of 90 arcsec is used. It is obvious that certain regions of the sky have been intensively studied at other wavelengths (empty regions in Fig. 15). In addition by comparing Fig. 15 with Fig. 5, it is evident that almost all of the brightest RBSC sources have already been identified.

The list of possible identification candidates as generated from cross-correlating the RBSC sources with various catalogues is intended to assist in determining the nature of the X-ray sources. No attempt was made to remove duplicate entries from different source catalogues and in some cases contradictory identification candidates may be given. With the help of X-ray parameters, such as the hardness ratios, the source extent and the f_X/f_{opt} ratio, a decision can be made as to which entry is the plausible

identification candidate (also see Motch et al. 1998 and Beuermann et al. 1999).

5. Electronic archive

All relevant information about access to the RBSC is available at <http://wave.xray.mpe.mpg.de/rosat/catalogues/rass-bsc>. The full catalogues (RBSC and identification catalogue) and the descriptions of the catalogue contents can be retrieved as ASCII files via the WWW or via anonymous ftp. The RBSC presents the X-ray data. Subsets of the catalogue sources may be retrieved via the ROSAT Source Browser also available at the above mentioned address. An example of a search inquiry and its output are explained in Figs. 16 – 17. The identification catalogue (Fig. 18 and Tab. 4) consists of the results from cross-correlating the RBSC with the catalogues listed in Tab. 3. The main X-ray properties (such as name, position in equatorial and galactic coordinates, and fluxes) are given, as well as a designated number which represents the number of counterpart candidates found within a search radius of 300 arcsec. For each of the candidates an individual record is appended, containing the source position, angular separation from the X-ray position, different magnitudes (or fluxes in Radio or IR wavelength bands), redshift, spectral type and classification (if available). The catalogues are meant to be living databases, so that whenever improved X-ray or new ID data are available they will be included. Each data record contains a date stamp according to year, month and day in which this record was changed or newly included.

Acknowledgements. We would like to thank the ROSAT team at MPE for their support and for stimulating discussions. We thank Damir Šimić for help in compiling the identification data and Ray Cruddace for the critical reading of the manuscript. The ROSAT Project is supported by the Bundesministerium für Bildung und Forschung (BMBF/DLR) and the Max-Planck-Gesellschaft (MPG). This work has made use of the SIMBAD database operated at CDS, Strasbourg, France. In addition this research also made use of the NASA/IPAC Extragalactic Database (NED), which is operated by the Jet Propulsion Laboratory, California Institute of Technology, under contract with NASA, and the COSMOS digitised optical survey of the southern sky, operated by the Royal Observatory Edinburgh and the Naval Research Laboratory, with support from NASA. We thank Richard MacMahon for making the APM catalogue available to MPE.

References

Abell G.O., Corwin H.G., Olowin R.P., 1989 ApJS 70, 1
 Alcalá J.M., Krautter J., Schmitt J.H.M.M., et al., 1995, A&AS 114, 109
 Alcalá J.M., Terranegra L., Wichmann R., et al., 1996, A&AS 119, 7
 Alcalá J.M., Chavarria C., Terranegra L., 1998, A&A 330, 1017
 Appenzeller I., Thiering I., Zickgraf F.-J., et al., 1998, ApJS 117, 319

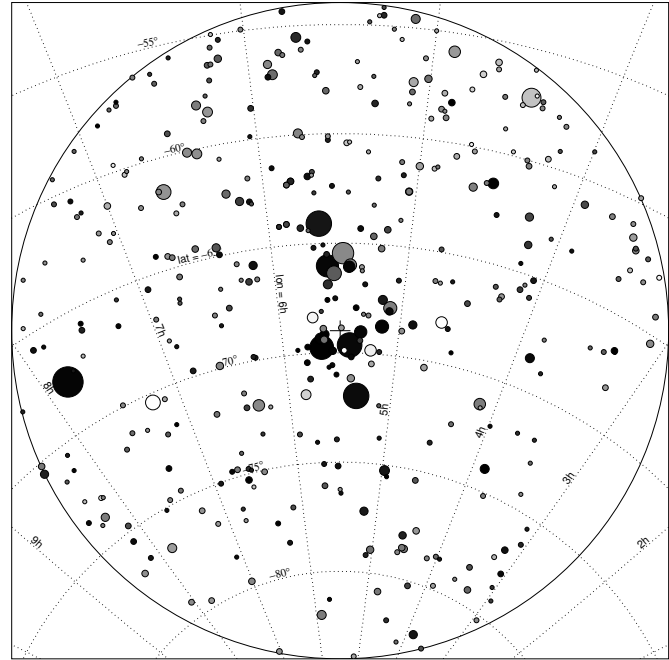


Fig. 17. Sample sky field plot of the search inquiry via the ROSAT source browser as used for Fig. 16. The size of the symbols is a function of the count-rate and the grey level corresponds to the hardness ratio HR1.

Aschenbach B., 1988, Appl. Optics 27, 1404
 Bade N., Engels D., Voges W., et al., 1998, A&AS 127, 145
 Berghöfer T.W., Schmitt J.H.M.M., Cassinelli J.P., 1996, A&AS 118, 481
 Böhringer H., Guzzo L., Collins C.A., et al., 1998, The Messenger 94, 21
 Beuermann K., Thomas H.-C., Reinsch K., et al., 1999, A&A, accepted
 Boller Th., Bertoldi F., Dennefeld M., Voges W., 1998, A&AS 129, 87
 Bowyer S., Lampton M., Lewis J., et al., 1996, ApJS 102, 129
 Buckley D.A.H., Sekiguchi K., Motch C., et al., 1995, MNRAS 275, 1028
 Burwitz V., Reinsch K., Schwöpe A.D., et al., 1996a, A&A 305, 507
 Burwitz V., Reinsch K., Beuermann K., Thomas H.-C., 1996b, A&A 310, L25
 Condon J.J., Cotton W.D., Greisen E.W., et al., 1998, AJ 115, 1693
 Covino E., Alcalá J.M., Allain S., et al., 1997, A&A 328, 187
 Cruddace R.G., Hasinger G.R., Schmitt J.H.M.M., 1987, in: Astronomy from Large Databases, Murtaugh F., Heck A. (eds.), p.177
 Danner R., 1998, A&AS 128, 331
 De Grandi S., Molendi S., Böhringer H., Chincarini G., Voges W., 1997, ApJ 486, 738
 Ebeling H., Voges W., Böhringer H., Edge A.C., 1993, A&A 275, 360
 Fleming T.A., 1998, ApJ 504, 461
 Fleming T.A., Molendi S., Maccacaro T., Wolter A., 1995, ApJS 99, 701

Table 4. Description of the columns of the identification table

RBSC row:

Col	abbreviation	description
1	SrcNam	the ROSAT All-Sky Survey Catalogue source name
2	R.A.	Right Ascension (2000) in decimal degrees
3	Dec.	Declination (2000) in decimal degrees
4	?p	the total positional error (1σ -radius) in arcsec, including $6''$ systematic error
5	# id	number of possible identification objects found within a search radius of 5 arcmin (= number of ID-rows following)
6	catalog-id	name of source catalogue (always 1RXS)
7	F	flag indicating the origin of the source position (always x: X-ray)
8	gal_Nh	galactic HI column density in units of 10^{21} atoms/cm ²
9	gal_long	galactic longitude l^{II} in decimal degrees
10	gal_lat	galactic latitude b^{II} in decimal degrees
11	hr1	hardness ratio 1 (as explained in Sect. 2.2.3.)
12	?hr1	error of hardness ratio 1
13	hr2	hardness ratio 2 (as explained in Sect. 2.2.3.)
14	?hr2	error of hardness ratio 2
15	ext	source extent in arcsec
16	exl	likelihood of source extent
17	srcl	likelihood of source detection defined as $\text{srcl} = -\ln P$ (P = probability that source is a spurious detection)
18	exp	exposure time in sec
19	src-cps	source count-rate (vignetting corrected) in the broad band in counts/sec
20	?src-cps	error of source count-rate in the broad band in counts/sec
21	flux1	X-ray flux 1 in the 0.1–2.4 keV energy range in $\text{erg cm}^{-2} \text{s}^{-1}$ (as explained in Sect. 3.3.5.)
22	flux2	X-ray flux 2 in the 0.1–2.4 keV energy range in $\text{erg cm}^{-2} \text{s}^{-1}$ (as explained in Sect. 3.3.5.)
23	t_obs_beg	first date (yymmdd.dd) of observation (.dd is the fraction of the day)
24	t_obs_end	last date (yymmdd.dd) of observation (.dd is the fraction of the day)
25	orgdat	date (yymmdd) when the source was included
26	moddat	date (yymmdd) when the source properties were changed

Identification row:

Col	abbreviation	description
1	source-ID	the source name
2	R.A.	Right Ascension (2000) in decimal degrees
3	Dec.	Declination (2000) in decimal degrees
4	sep	the positional separation between RBSC source and ID object in arcsec
5	pa	the position angle (North to East) between RBSC source and ID object in degrees
6	catalog-id	name of source catalogue
7	F	flag indicating the origin of the source position (o: optical; x: X-ray; r: Radio; e: EUV; i: IR)
8	type	type or class of object
9	fxfopt	ratio of X-ray to optical flux f_x/f_{opt}
10	vmag	visual magnitude
11	bmag	blue magnitude
12	rmag	red magnitude
13	b-r	(blue–red) colour
	hr1	or hardness ratio 1 if entry is from ROSATP3 or ROSATWGA catalogue
14	b-v	(blue–visual) colour
	?hr1	or error of hardness ratio 1 if entry is from ROSATP3 or ROSATWGA catalogue
15	u-b	(ultraviolet–blue) colour
	hr2	or hardness ratio 2 if entry is from ROSATP3 or ROSATWGA catalogue
16	var	variability flag
	?hr2	or error of hardness ratio 2 if entry is from ROSATP3 or ROSATWGA catalogue
17	red-sh.	red-shift
	ext, exl	or source extent in arcsec and likelihood of source extent if entry is from ROSATP3 catalogue
18	dist	distance in kpc
	snr	or signal-to-noise-ratio if FIRST entry
	srcl, exp	or likelihood (ROSATP3) or signal-to-noise-ratio (ROSATWGA/ROSHRI) of source detection and exposure in sec if entry is from ROSAT pointing catalogues
19	IR-12mu	infrared flux in the 12 μm band if entry is from IRAS catalogues IRASFSC and IRASPSC
	R-f6cm	or Radio flux in the 6cm band if entry is from VERONV8 catalogue
	Ned-flux	or Radio (IR) flux density in mJy in the frequency (wavelength in microns) band given in column 20 if entry is from NED
20	IR-25mu	infrared flux in the 25 μm band if entry is from IRAS catalogues IRASFSC and IRASPSC
	R-f11cm	or Radio flux in the 11cm band if entry is from VERONV8 catalogue
	fl-band	or frequency (wavelength in microns) band used for flux given in column 19 if entry is from NED
	src-cps	or source count-rate (vignetting corrected) in the broad band in counts/sec if entry is from ROSAT pointing catalogues
21	IR-60mu	infrared flux in the 60 μm band if entry is from IRAS catalogues IRASFSC and IRASPSC
	R-f20cm(I)	or Radio integrated flux density in mJy in the 20cm band if entry is from FIRST or NVSS catalogues
	?src-cps	or error of source count-rate in the broad band in counts/sec if entry is from ROSAT pointing catalogues
22	IR-100mu	infrared flux in the 100 μm band if entry is from IRAS catalogues IRASFSC and IRASPSC
	R-f20cm(P)	or Radio peak flux density in mJy in the 20cm band if entry is from FIRST or NVSS catalogues
	size	or size of object in arcmin if entry is from NED
	roff	or off-axis angle in arcmin if entry is from ROSAT pointing catalogues
23	comments	additional information concerning type or class of object
24	orgdat	date (yymmdd) when the source was included
25	moddat	date (yymmdd) when the source properties were changed

- Fleming T.A., Snowden S.L., Pfeffermann E., Briel U., Greiner J., 1996, A&A 316, 147
- Forman W., Jones C., Cominsky L., et al., 1978, ApJS 38, 357
- Gregory P.C., Condon J.J., 1991, ApJS 75, 1011
- Gregory P.C., Scott W.K., Douglas K., Condon J.J., 1996, ApJS 103, 427
- Haberl F., Thorstensen J.R., Motch C., et al., 1994, A&A 291, 171
- Haberl F., Motch C., 1995, A&A 297, L37
- Hakala P.J., Watson M.G., Vilhu O., et al., 1993, MNRAS 263, 61
- Harris D.E., Forman W., Gioia I.M., et al., 1994, SAO HEAD CD-ROM Series I (Einstein), Nos 18-36
- Hasinger G., Trümper J., Schmidt M., 1991, A&A 246, 2
- Helou G., Madore B.F., Schmitz M., et al., 1995, in: Information and On-Line Data in Astronomy, Egret D. & Albrecht M.A. (eds.) (Dordrecht: Kluwer), p.95
- Hoffleit D., Warren Jr W.H., 1991, Astronomical Data Center, NSSDC/ADC
- Høg E., Kuzmin A., Bastian U., et al., 1998, A&A 335, L65
- Hünsch M., Schmitt J.H.M.M., Voges W., 1998a, A&AS 127, 251
- Hünsch M., Schmitt J.H.M.M., Voges W., 1998b, A&AS 132, 155
- Hünsch M., Schmitt J.H.M.M., Sterzik, M.F., Voges W., 1999, A&AS 135, 319
- IRAS Catalogs and Atlases Explanatory Supplement, 1988, Beichman C., Neugebauer G., Habing H.J., Clegg P.E., and Chester T.J. (eds.) (Washington, DC: GPO), NASA RP-1190
- Kent B.J., Reading D.H., Swinyard B.M., Graper E.B., Spurett P.H., 1990, Proc. SPIE, 1344, 255
- Kock A., 1998, PhD thesis, Universität Würzburg
- Kock A., Meisenheimer K., Fürst E., et al., 1996, A&A 307, 745
- Krautter J., Wichmann R., Schmitt J.H.M.M., et al., 1997, A&AS 123, 329
- Kunkel M., 1997, PhD thesis, Universität Würzburg
- Lasker B.M., Sturch C.R., McLean B.J., et al., 1990, AJ 99, 2019
- Laurent-Muehleisen S.A., Kollgaard R.I., Ciardullo R., et al., 1998, ApJS 118, 127
- Law-Green J.D.B., Leahy J.P., Alexander P., et al., 1995, MNRAS 274, 939
- Levine A., Lang F., Lewin W., Primini F., Dobson C. 1984, ApJS 54, 581
- Maccacaro T., Gioia I.M., Wolter A., et al., 1988, ApJ 326, 680
- MacGillivray H.T., Stobie R.S., 1985, Vistas in Astronomy, vol 27, 433
- Magazzu A., Martin E.L., Sterzik M.F., et al., 1997, A&AS 124, 449
- Markert T., Winkler P., Laird F., et al., 1979, ApJS 39, 573
- Mason K.O., Watson M.G., Ponman T.J., et al., 1992, MNRAS 258, 749
- Mason K.O., Hassall B.J.M., Bromage G.E., et al., 1995, MNRAS 274, 1194
- McHardy I., Lawrence A., Pye J., Pounds K., 1981, MNRAS 197, 893
- McMahon R.G., Irwin M.J., 1992, in: Digitised Optical Sky Surveys, MacGillivray H.T. and Thomson E.B. (eds.), p.417
- Metanomski A.D.F., Pasquini L., Krautter J., Cutispoto G., Fleming T.A. 1998, A&AS 131, 197
- Moshir M., Copan G., Conrow T, et al., 1989, Infrared Processing and Analysis Center
- Motch C., Guillout P., Haberl F., et al., 1997a, A&AS 122, 201
- Motch C., Haberl F., Guillout P., et al., 1996, A&A 307, 459
- Motch C., Haberl F., Dennerl K., Pakull M., Janot-Pacheco E., 1997b, A&A 323, 853
- Motch C., Guillout P., Haberl F., et al., 1998, A&AS 132, 341
- Nass P., Bade N., Kollgaard R. I., et al., 1996, A&A 309, 419
- Neuhäuser R., Sterzik M.F., Schmitt J.H.M.M., Wichmann R., Krautter J., 1995, A&A 297, 391
- Neuhäuser R., Torres G., Sterzik M.F., Randich S., 1997, A&A 325, 647
- Nugent J., Jensen K., Nousek J., et al., 1983, ApJS 51, 1
- Perlman E., Stocke J.T., Schachter J., et al. , 1996, ApJS 104, 251
- Pfeffermann E., Briel U.G., Hippmann H., et al., 1988, Proc. SPIE, 733, 519
- Pye J.P., McGale P.A., Allan D.J., et al., 1995, MNRAS 274, 1165
- Ritter H., Kolb U., 1998, A&AS 129, 83
- Romer A.K., Collins C.A., Böhringer H., et al., 1994, Nat 372, 75
- Schmitt J.H.M.M., Fleming T.A., Giampapa M.S., 1995, ApJ 450, 392
- Schmitt J.H.M.M., 1997, A&A 318, 215
- Schwöpe A., Hasinger G., Lehmann I., et al., 1999, to be submitted
- Snowden S.L., Freyberg M.J., Schmitt J.H.M.M., et al., 1995, ApJ 454, 643
- Snowden S.L., Egger R., Freyberg M.J., et al., 1997, ApJ 485, 125
- Stark A.A., Gammie C.F., Wilson R.W., et al., 1992, ApJS 79, 77
- Staubert R., König M., Friedrich S., et al., 1994, A&A 288, 513
- Stern R.A., Schmitt J.H.M.M., Kahabka P.T., 1995, ApJ 448, 683
- Thomas H.-C., Beuermann K., Schwöpe A.D., Burwitz V., 1996, A&A 313, 833
- Thomas H.-C., Beuermann K., Reinsch K., et al., 1998, A&A 335, 467
- Trümper J., 1983, Adv. Space Res. 27, 1404
- Trümper J., Hasinger G., Aschenbach B. et al. 1991, Nature, 349, 579
- Veron-Cetty M.P., Veron P., 1998, ESO Scientific Report 18
- Voges W., Aschenbach B., Boller Th., et al., 1996a, IAUC 6420
- Voges W., Boller Th., Dennerl K., et al., 1996b, in: Proc. of the Conference *Röntgenstrahlung from the Universe*, MPE Report 263, p.637
- Voges W., Boller Th., 1998, Astron. Nachr. 319, 3
- Walter R, Fink H.H., A&A 274, 105, 1993
- Warwick R., Marshall N., Fraser G., et al., 1981, MNRAS 197, 865
- Wells A., Abbey A.F., Barstow M.A., et al., 1990, Proc. SPIE, 1344, 230
- White N.E., Giommi P., Angelini L., 1994, IAUC 6100
- White R.L., Becker R.H., Helfand D.J., Gregg M.D., 1997, ApJ 475, 479

- Wichmann R., Krautter J., Schmitt J.H.M.M., et al., 1996, A&A 312, 439
- Wichmann R., Sterzik M.F., Krautter J., Metanomski A., Voges W., 1997, A&A, 326, 211
- Wiedenmann G., Scheingraber H., Voges W., 1997, in: Data Analysis in Astronomy, Di Gesu V., Duff M.J.B., Heck A., Maccacron M.C., Scarsi L., & Zimmermann H.U. (eds.), p.203
- Wood K., Meekins J., Yentis D., et al., 1984, ApJS 56, 507
- Xie G., Cha G., Bai J., et al., 1997, Acta Astron. Sin. 17, 323
- Yentis D.J., Cruddace R.G., Gursky H., et al, 1992, in: Digitised Optical Sky Surveys, MacGillivray H.T. and Thomson E.B. (eds.), p.67
- Zimmermann H.U., Becker W., Belloni T., et al., 1994, MPE Report 257